

Accretion-disc precession in UX Ursae Majoris

E. de Miguel,^{1,2} ^{*} J. Patterson,³ D. Cejudo,⁴ J. Ulowetz,⁵ J. L. Jones,⁶
 J. Boardman,⁷ D. Barret,⁸ R. Koff,⁹ W. Stein,¹⁰ T. Campbell,¹¹
 T. Vanmunster,¹² K. Menzies,¹³ D. Slauson,¹⁴ W. Goff,¹⁵ G. Roberts,¹⁶
 E. Morelle,¹⁷ S. Dvorak,¹⁸ F.-J. Hamsch,¹⁹ D. Starkey,²⁰ D. Collins,²¹
 M. Costello,²² M. J. Cook,²³ A. Oksanen,²⁴ D. Lemay,²⁵ L. M. Cook,²⁶
 Y. Ogmen,²⁷ M. Richmond,²⁸ and J. Kemp²⁹

¹ Departamento de Física Aplicada, Facultad de Ciencias Experimentales, Universidad de Huelva, 21071 Huelva, Spain

² CBA-Huelva, Observatorio del CIECEM, Parque Dumar, Matalascañas, 21760 Almonte, Huelva, Spain

³ Department of Astronomy, Columbia University, 550 West 120th Street, New York, NY 10027, USA

⁴ CBA-Madrid, Camino de las Canteras 42, Buzón 5, La Pradera del Amor, El Berrueco, 28192 Madrid, Spain

⁵ CBA-Illinois, Northbrook Meadow Observatory, 855 Fair Lane, Northbrook, IL 60062, USA

⁶ CBA-Oregon, Jack Jones Observatory, 22665 Bents Road NE, Aurora, OR, USA

⁷ CBA-Wisconsin, Luckydog Observatory, 65027 Howath Road, de Soto, WI 54624, USA

⁸ CBA-France, 6 Le Marouzeau, St Leger Bredereix, 2300, France

⁹ CBA-Colorado, Antelope Hills Observatory, 980 Antelope Drive West, Bennett, CO 80102, USA

¹⁰ CBA-Las Cruces, 6025 Calle Paraiso, Las Cruces, NM 88012, USA

¹¹ CBA-Arkansas, 7021 Whispering Pine Road, Harrison, AR 72601, USA

¹² CBA-Belgium, Walhostraat 1A, B-3401 Landen, Belgium

¹³ CBA-Massachusetts, 318A Potter Road, Framingham, MA 01701, USA

¹⁴ CBA-Iowa, Owl Ridge Observatory, 73 Summit Avenue NE, Swisher, IA 52338, USA

¹⁵ CBA-California, 13508 Monitor Lane, Sutter Creek, CA 95685, USA

¹⁶ CBA-Tennessee, 2007 Cedarwood Drive, Franklin, TN 37067, USA

¹⁷ CBA-France, 9 Rue Vasco de Gama, 59553 Lauwin Planque, France

¹⁸ CBA-Orlando, Rolling Hills Observatory, 1643 Nightfall Drive, Clermont, FL, USA

¹⁹ CBA-Mol, Andromeda Observatory, Oude Bleken 12, B-2400 Mol, Belgium

²⁰ CBA-Indiana, DeKalb Observatory H63, Auburn, IN 46706, USA

²¹ College View Observatory, Warren Wilson College, Asheville, NC, USA

²² CBA-Fresno, 1125 East Holland Avenue, Fresno, CA 93704, USA

²³ CBA-Newcastle, 9 Laking Drive, Newcastle, Ontario, Canada

²⁴ CBA-Finland, Hankasalmi Observatory, Verkkoniementie 30, FI-40950 Muurame, Finland

²⁵ 195 Rang 4 Ouest, St-Anaclet, QC, Canada G0K 1H0, Canada

²⁶ CBA-Concord, 1730 Helix Court, Concord, CA 94518, USA

²⁷ CBA-Cyprus, Green Island Observatory (B34), Gecitkale, North Cyprus

²⁸ Physics Department, Rochester Institute of Technology, Rochester, NY 14623, USA

²⁹ Department of Physics, Middlebury College, Middlebury, VT 05753, USA

31 December 2015

ABSTRACT

We report the results of a long campaign of time-series photometry on the nova-like variable UX Ursae Majoris during 2015. It spanned 150 nights, with ~ 1800 hours of coverage on 121 separate nights. The star was in its normal ‘high state’ near magnitude $V = 13$, with slow waves in the light curve and eclipses every 4.72 hours. Remarkably, the star also showed a nearly sinusoidal signal with a full amplitude of 0.44 mag and a period of 3.680 ± 0.007 d. We interpret this as the signature of a retrograde precession (wobble) of the accretion disc. The same period is manifest as a ± 33 s wobble in the timings of mid-eclipse, indicating that the disc’s centre of light moves with this period. The star also showed strong ‘negative superhumps’ at frequencies $\omega_{\text{orb}} + N$ and $2\omega_{\text{orb}} + N$, where ω_{orb} and N are respectively the orbital and precession frequencies. It is possible that these powerful signals have been present, unsuspected, throughout the more than 60 years of previous photometric studies.

Key words: accretion, accretion discs – binaries: close – novae, cataclysmic variables – Stars: individual: UX Ursae Majoris.

1 INTRODUCTION

UX Ursae Majoris (UX UMa) is one of the oldest and most thoroughly studied of the cataclysmic variables (CVs). Among non-eruptive CVs, it's probably the champion in both respects. Visual and photoelectric photometry showed it to be an eclipsing binary with a remarkably short period of 4.72 hours (Zverev & Kukarkin 1937; Johnson, Perkins & Hiltner 1954; Krzeminski & Walker 1963), and Walker & Herbig (1954) proposed a model in which the hot star in the binary is surrounded by a large ring of gas on which a bright region (hot spot) resides. The hot spot became a key feature of the basic model for understanding CVs, in which the spot is interpreted as the region where the mass-transfer stream impacts the outer edge of the accretion disc.

The spectrum of UX UMa closely resembles that of dwarf novae in eruption: a blue continuum with broad, shallow hydrogen absorption lines, and narrow H emission contained within these absorption troughs. He I and weak He II emission are sometimes also present. Recent spectroscopic studies have been reported by Linnel et al. (2008) and Neustroev et al. (2011). The distance is 345 ± 34 pc (Baptista et al. 1995, 1998). The out-of-eclipse mean V magnitude is ~ 13.0 , but this is adversely affected by interstellar extinction (~ 0.2 mag) and the geometrical projection of a fairly edge-on disc (~ 1.0 mag; Paczynski & Schwarzenberg-Czerny 1980). After these corrections, the angle-averaged $\langle M_V \rangle$ is about $+4.1$. That's just about right for the 'high state' of a dwarf nova with an orbital period of 4.7 hours (Fig. 1 of Patterson 2011). Thus the spectrum and brightness are consistent with interpretation as a dwarf nova in the high state.

In addition, UX UMa shows another phenomenon which is highly characteristic of dwarf novae: very rapid (~ 30 s) oscillations in its optical and UV brightness (Warner & Nather 1972; Nather & Robinson 1974; Knigge et al. 1998a). These oscillations are seen in practically every dwarf nova near the peak of eruption, and are consequently called 'dwarf nova oscillations' (DNOs; Patterson 1981, especially the abstract and Fig. 17). Their presence in UX UMa is yet another reason why the star is commonly regarded, and described, as essentially a 'permanently erupting dwarf nova'.

UX UMa vaulted to the world's attention from a program of time-series photometry in the 1940s. We launched a more intensive program in 2015, and discovered several additional periodic signals, which we describe in this paper and interpret as signifying the retrograde precession of the accretion disc.

2 OBSERVATIONS

We conducted this campaign with our global network of small photometric telescopes, the Center for Backyard Astrophysics (CBA). The network's general approach to instrumentation and observing methods is given by Skillman & Patterson (1993), and the summary observing log is given in Table 1. We used differential photometry with respect to one of the nearby field stars GSC 3469-0356 ($V = 13.068$), GSC 3469-0290 ($V = 13.370$), and GSC 3469-0867 ($V = 13.497$), with magnitudes corresponding to the

Table 1. Log of observations.

Observer	CBA station	Nights/hours
Cejudo	Madrid (Spain) 0.3 m	59/259
Ulowetz	Illinois (USA) 0.24 m	53/216
de Miguel	Huelva (Spain) 0.3 m	31/173
Jones	Oregon (USA) 0.35 m	16/126
Boardman	Wisconsin (USA) 0.3 m	19/104
Barrett	Le Marouzeau (France) 0.2 m	24/99
Koff	Colorado (USA) 0.25 m	14/95
Stein	Las Cruces (New Mexico, USA) 0.35 m	12/85
Campbell	Arkansas (USA) 0.15 m	15/76
Vanmunster	Belgium 0.35 m	14/63
Menzies	Massachusetts (USA) 0.35 m	9/60
Slauson	Iowa (USA) 0.24 m	15/59
Goff	Sutter Creek (California, USA) 0.5 m	9/48
Roberts	Tennessee (USA) 0.4-0.5 m	8/45
Morelle	France 0.3 m	6/43
Dvorak	Rolling Hills (Orlando, USA) 0.25 m	8/38
Hamsch	Belgium 0.28 m	7/29
Starkey	Auburn (Indiana, USA) 0.4 m	4/28
Collins	North Carolina (USA) 0.35 m	6/25
Costello	Fresno (USA) 0.35 m	4/21
M. Cook	Newcastle (Ontario, Canada) 0.4 m	4/20
Oksanen	Finland 0.4 m	3/20
Lemay	Quebec (Canada) 0.35 m	7/24
L. Cook	Concord (California, USA) 0.2-0.7 m	4/12
Ogmen	Cyprus 0.35 m	2/10
Richmond	Rochester (New York, USA) 0.30 m	2/7

APASS photometric survey (Henden et al. 2012). We constructed light curves using overlaps of the various time series to calibrate each on a common instrumental scale. That scale is roughly a V magnitude since most of our data is unfiltered in order to improve signal-to-noise. Nevertheless, we did obtain sufficient data with a true V filter to measure offsets, and this allowed us to place all our data into a magnitude scale that is expected to nearly correspond to a true V , with a zero-point uncertainty of ~ 0.04 mag.

The cycle time (integration + readout) between points in the various time series was usually near ~ 60 seconds. We made no correction for differential (color) extinction, although such a correction is in principle necessary, since all CVs are bluer than field stars. But in a long time series, such effects are always confined to the same frequencies (very near 1 and 2 cycles per sidereal day), so the resultant corruption is easily identified and ignored. In the present case, it is also mitigated by the northern latitudes of observers and the far-northern declination of the star (51 degrees), which made it possible to obtain long runs within our self-imposed limit of 2.0 airmasses. Finally, we just prefer to keep human hands off the data as much as possible.

As detailed in Table 1, the campaign amounted to 355 separate time series on 121 nights distributed over a span of 153 nights from February 24 to July 26, 2015. The total coverage was 1785 hours, all from sites in Europe and North America. This longitude span permitted many ~ 14 hour runs, which eliminated all possibility of daily aliases – the usual bugaboo of single-longitude time series.

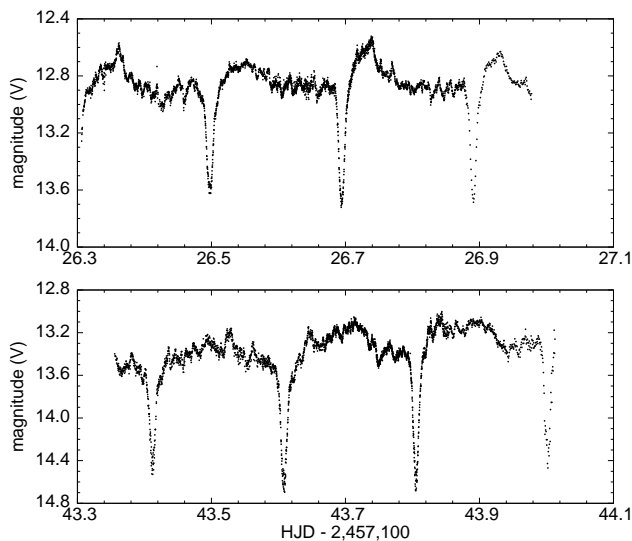


Figure 1. Representative light curves of UX UMa on two nights in the 2015 campaign.

3 LIGHT CURVES AND ECLIPSES

Two representative nightly light curves are shown in Fig. 1. They are similar to essentially all light curves in the literature (e.g. Johnson, Perkins & Hiltner 1954; Walker & Herbig 1954; Warner & Nather 1972): regular, asymmetric eclipses, with ingress being steeper than egress; irregular, non-coherent variations at short timescales (flickering); plus a roughly ‘orbital’ hump, although the latter varies markedly – and interestingly! – from one night to the next. The mean brightness outside the eclipses and at minimum are $V = 13.02$ and $V = 13.94$, respectively. These values are far from constant, and vary from one orbital cycle to the next. The upper frame of Fig. 2 shows a sample 27-day light curve, which suggests the presence of a slow wave with a period near 3.7 d that modulates the out-of-eclipse brightness, as well as the magnitude of the system at mid-eclipse. And the bottom frame shows a 100-day light curve (with eclipses removed), which confirms the apparent stability of this slow wave.

We measured the time of minimum eclipse and the corresponding magnitude by fitting a parabolic function to the bottom half of the minimum (± 0.04 in orbital phase). Individual errors were estimated by Monte Carlo methods and found to vary in the range $(0.7\text{--}6) \times 10^{-4}$ d, with median value of 2×10^{-4} d. Strictly speaking, this fitting procedure provides estimates of the time of minimum light, which tends to occur slightly later than the time of mid-eclipse in UX UMa (Baptista et al. 1995). But our data do not allow us to discriminate between these two timings, since the differences are much smaller than our uncertainties. A total of 214 minima were timed. These times, collected in Table 2, were found to track the ephemeris

$$T_{\min}(\text{HJD}) = 2,457,078.51002(6) + 0.19667118(19)E. \quad (1)$$

Not surprisingly, the corresponding $O-C$ residuals were found to show no statistically significant departure from linearity over the ~ 150 d baseline, since the orbital modulation is expected to be a stable clock on this time scale. But as

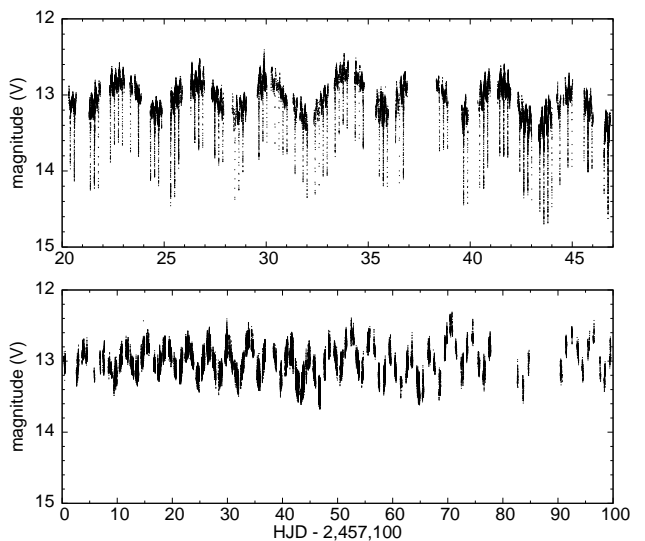


Figure 2. *Upper frame:* a 27-day light curve, showing eclipses, possibly ‘orbital’ humps, and a candidate ~ 3.7 d variation (also apparent in the eclipse minima). *Lower frame:* the central 100 days of the campaign, with eclipses removed. The ~ 3.7 d variation seems to endure throughout.

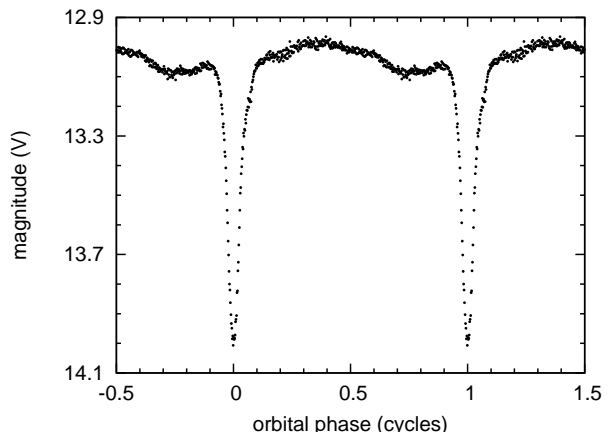


Figure 3. Mean orbital light curve over the full 5-month campaign. The mean out-of-eclipse magnitude is $V = 13.02$ mag and the mean eclipse depth is 0.92 mag. Maximum light occurs near orbital phase 0.35.

we shall see below, they appear to be modulated by the 3.7 d period described above.

The orbital light curve is significantly contaminated by flickering, the 3.7 d modulation, and the ‘superhump’ variations described below. Making no attempt to remove these effects, and simply averaging over the ~ 1800 hours of coverage, we found the mean orbital light curve seen in Fig. 3. This appears to be the first mean orbital light curve published for this venerable, oft-observed star. And it shows maximum light near orbital phase 0.35, roughly 180° out of phase with the standard ‘hot spot’ model developed for U Geminorum, and thought to prevail, *mutatis mutandis*, in all CVs (Smak 1971; Warner & Nather 1971). The accretion geometry must be significantly different in UX UMa.

Table 2. Timings of mid-eclipse (HJD – 2,457,000).

78.5100	78.7067	79.6903	81.8535	83.6238	83.8202	84.6072	88.5405	88.7371	89.7204
91.8847	93.6535	93.8504	95.8169	96.6035	97.5871	98.5704	99.3574	99.5543	99.7508
100.3406	100.5373	102.7010	102.8974	103.6839	103.8804	104.4702	105.8460	106.8306	107.4204
107.6177	108.4037	108.6006	108.7971	108.9946	109.3872	109.5843	109.7808	109.7807	109.9780
110.3708	110.5677	110.7644	111.7466	111.9439	112.3373	112.5341	112.7302	112.9277	113.5175
113.7146	114.5015	114.6975	114.8945	115.4837	116.6632	116.8615	117.6474	117.8443	118.4344
118.6303	119.4173	119.6142	119.8106	120.4012	120.5982	121.3848	121.5817	121.7782	122.3679
122.5644	122.7605	122.9570	123.3509	123.7435	124.3346	124.5313	124.7283	125.3184	125.5147
125.7115	126.4977	126.6944	126.8909	127.4810	127.6765	128.4647	128.6618	128.8575	129.6447
129.8404	130.4308	130.6275	130.8235	131.0210	131.4147	131.8079	132.0053	132.3981	132.5946
132.7920	132.9887	133.3812	133.5772	133.7745	133.9711	134.3641	134.5612	134.7576	135.5452
135.7413	135.9382	136.5286	136.7253	138.4939	138.6909	138.8884	139.6751	139.8719	140.4620
140.6585	140.8542	141.4447	141.6413	141.8378	142.4276	142.6249	142.8214	143.4122	143.6082
143.8053	144.0018	144.3949	144.7883	145.7714	145.9683	146.7553	147.7391	148.5249	149.5079
149.7052	150.4920	150.6885	150.8851	151.4758	151.6720	152.4582	152.8514	153.4418	153.6377
153.8349	154.4253	154.6217	155.4089	155.6054	155.8012	156.5882	156.7845	157.5718	158.5556
159.5390	160.5210	162.4896	163.4720	164.4554	164.8488	165.4389	166.4216	166.6187	166.8156
167.4055	167.6011	168.3887	168.5853	169.5697	169.7657	170.5522	170.7485	171.5346	172.5197
173.5027	175.4691	175.6662	176.6494	177.4359	177.6320	183.7289	184.7127	190.4157	190.6130
191.4001	192.5786	193.5618	194.5464	195.7266	196.5122	197.6937	198.4796	199.4623	201.6262
201.8226	202.4132	203.7890	206.5436	208.5088	209.4941	209.6898	211.6558	221.4904	222.4728
223.4569	224.4399	227.3903	227.7846						

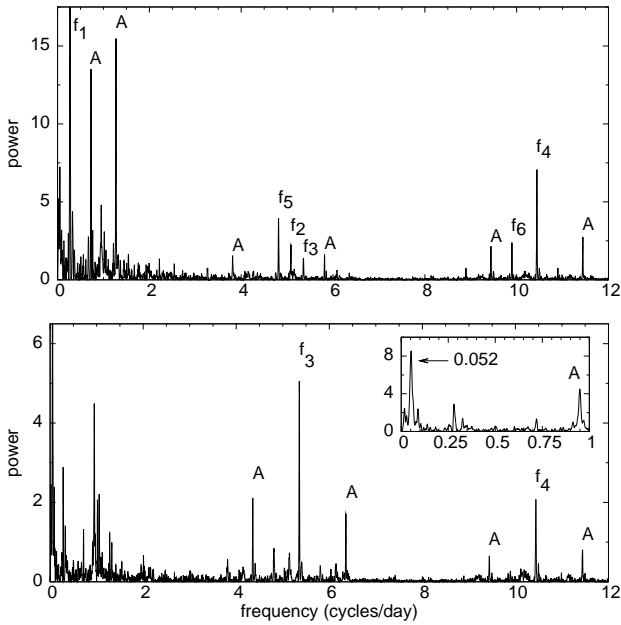


Figure 4. *Upper frame:* power spectrum of the full, 5-month light curve (with eclipses removed). The most prominent peaks are labeled f_1 through f_6 , and one-day aliases are designated ‘A’. There are only two independent (unrelated) frequencies: the strong signal $f_1 = 0.2717 \text{ c d}^{-1}$ (nodal, N), which rises off-scale to a power of 43.5 (or semi-amplitude of 0.22 mag); and f_2 , which corresponds to the orbital frequency, ω_{orb} . *Lower frame:* power spectrum of the residual light curve, after the nodal and orbital frequencies are subtracted. The two obvious peaks (f_3 and f_4) occur at $\omega_{\text{orb}} + N$ and $2\omega_{\text{orb}} + N$, and correspond to ‘negative superhumps’. The strong peaks labeled f_5 and f_6 in the upper frame coincide with $\omega_{\text{orb}} - N$ and $2\omega_{\text{orb}} - N$. These probably arise from modulation of the orbital signal by N , and their amplitude is greatly reduced after the subtraction. Inset is a zoom-in of the power spectrum in the range $0\text{--}1 \text{ c d}^{-1}$ showing a possible detection at $0.0521(8) \text{ c d}^{-1}$ (see text for details).

4 PERIODIC SIGNALS IN THE LIGHT CURVE

Our primary analysis tool for studying periodic waves is power spectra calculated by Fourier methods. The frequency analysis was performed by using the PERIOD04 package (Lenz & Breger 2005), based on the discrete Fourier transform method. Uncertainties in the frequencies and amplitudes were estimated by using Monte Carlo methods from the same package. Of course the sharp eclipses severely contaminate analysis by Fourier methods, since the latter represent time series as sums of sinusoids. So to prepare the light curves for study, we first removed the eclipse portion of the light curves, viz. the phase interval 0.9–1.1.

The low-frequency region of the power spectrum is shown in the upper frame of Fig. 4, where the most prominent peaks are labeled f_1 through f_6 , and alias peaks marked with ‘A’. In the figure, and throughout the paper, frequencies are expressed in cycles per day,¹ for which we use c d^{-1} as a shorthand. A prominent peak (f_2 in Fig. 4) is observed at $5.0847(9) \text{ c d}^{-1}$. This signal, with a semi-amplitude of 0.042 mag, coincides with the orbital frequency ω_{orb} . But the most powerful signal (f_1 in Fig. 4) occurs at $0.2717(5) \text{ c d}^{-1}$, or $3.680(3) \text{ d}$, a signal that is unrelated to the orbital motion, and that we denote as N , in anticipation of identifying it with nodal precession of the accretion disc. We summed at 0.2717 c d^{-1} , and found a highly sinusoidal waveform with a semi-amplitude of 0.22 mag. This is shown in the upper frame of Fig. 5.

In addition to ω_{orb} and N , other signals appear in the vicinity of ω_{orb} and $2\omega_{\text{orb}}$. For their characterization, we subtracted the sinusoids corresponding to N and ω_{orb} from the full out-of-eclipse data set, and then recalculated the power spectrum of the residual light curve. The results are shown in the lower frame of Fig. 4, which reveals obvious signals at

¹ The natural frequency unit for time-series studies on a planet plagued by rotation and sunrise.

Table 3. The most significant frequencies, along with their semi-amplitudes (A) and physical interpretation.

label	frequency (c d^{-1})	A (mag)	meaning
f_1	0.2717(5)	0.220(1)	N (nodal)
f_2	5.0847(9)	0.042(1)	ω_{orb} (orbital)
f_3	5.3562(4)	0.069(1)	$\omega_{\text{orb}} + N$ (nsh)
f_4	10.4391(4)	0.034(1)	$2\omega_{\text{orb}} + N$ (nsh)
f_5	4.814(4)		$\omega_{\text{orb}} - N$
f_6	9.899(4)		$2\omega_{\text{orb}} - N$

5.3562(4) and 10.4391(4) c d^{-1} (f_3 and f_4 in Fig. 4), with semi-amplitudes of 0.069 and 0.034 mag, respectively. These are consistent with identifications as $\omega_{\text{orb}} + N$ and $2\omega_{\text{orb}} + N$, which are expected at 5.3564(7) and 10.4410(9) c d^{-1} , respectively. These upper sidebands of the orbital frequency are known as *negative superhumps* in variable-star nomenclature, because in period (rather than frequency) language, their period excesses over P_{orb} , $P_{\text{orb}}/2$, etc. are *negative*.² The mean waveform of these negative superhumps are shown in the lower frame of Fig. 5.

The transition from the upper to the lower frame in Fig. 4 looks odd. Of course the one-day aliases, along with the main peaks, disappear when the N and ω_{orb} signals are subtracted from the time series. But in Fig. 4 there are also strong peaks at 4.814(1) and 9.899(1) c d^{-1} (f_5 and f_6 in Fig. 4), with amplitudes greatly reduced after the subtraction. That’s surprising. But these frequencies are essentially equal to $\omega_{\text{orb}} - N$ and $2\omega_{\text{orb}} - N$, so a good possibility is that the dominant N signal severely modulates the orbital signal, producing artificial flanking peaks at $\pm N$. The effects described below in §5 support this. Only the higher-frequency $+N$ sidebands – the negative superhumps – survive the subtraction. A summary of the main frequencies is given in Table 3.

The power spectrum in the lower frame of Fig. 4 seems to show a strong broad peak around 1 c d^{-1} . This peak, centred around 0.948(2) c d^{-1} , is actually an alias of a stronger detection at 0.0521(8) c d^{-1} , as shown inset in a zoomed-in view of the power spectrum in the range 0–1 c d^{-1} . Is this detection an indication of a ~ 19 day periodicity in UX UMa? It could be, but after a closer inspection we find no trace of this signal during, approximately, the first half of the campaign. Admittedly, we have no grounds for believing that this is a true detection, and we are more inclined to guess that it is just noise.

The waveforms of all four physically significant signals (N , ω_{orb} , $\omega_{\text{orb}} + N$, $2\omega_{\text{orb}} + N$) are impressively sinusoidal, and probably indicate that none of these signals rely on the deep eclipse for their existence. UX UMa would probably show these effects at any binary inclination, although the amplitude may well depend on inclination.

² The terminology goes back to Harvey et al. (1995), and the full suite of CV periodic-signal arcana is reviewed in Appendix A of Patterson et al. (2002).

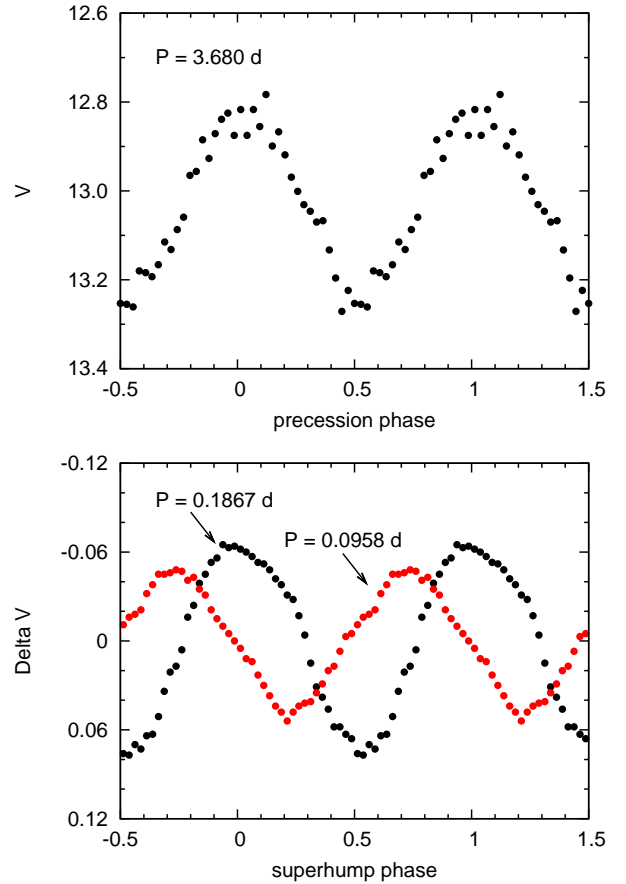


Figure 5. *Upper frame:* mean light curve folded on the nodal (N) frequency (0.2717 c d^{-1} or 3.68 d) relative to the ephemeris given in Eq. (2). *Lower frame:* mean light curve after removing the nodal and orbital signals folded on the $\omega_{\text{orb}} + N$ frequency (5.3562 c d^{-1} or 0.1867 d, black points) and the $2\omega_{\text{orb}} + N$ frequency (10.4391 c d^{-1} or 0.0958 d, red points) relative to the ephemeris given in Eq. (3).

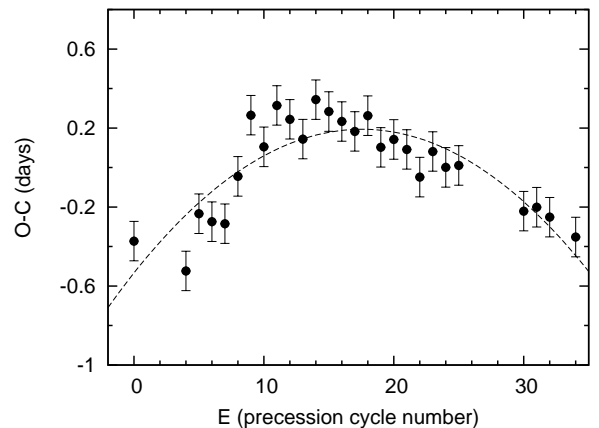
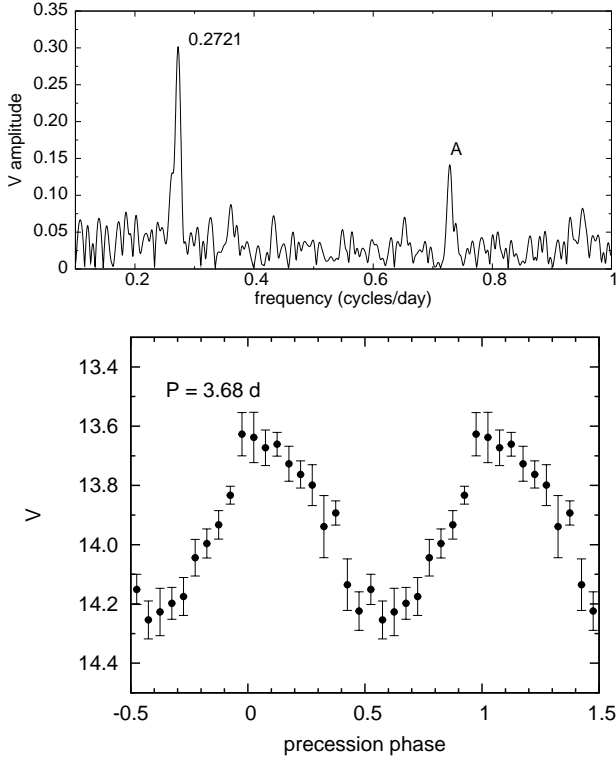


Figure 6. $O - C$ residuals of the timings of maximum light (Table 4) on the 3.68 day cycle as determined from the ephemeris given in Eq. (2). The dashed curve represents the best quadratic fit, from which we infer that the nodal period changes by ~ 0.2 d over the 5-month campaign.

Table 4. Times of maximum light on the 3.68 day cycle (HJD – 2,457,000).

81.64	96.25	100.23	103.88	107.56	111.49	115.49
119.02	122.92	126.54	130.13	134.02	137.65	141.29
144.93	148.70	152.23	155.96	159.60	163.15	166.97
170.58	174.28	192.50	196.21	199.85	207.13	

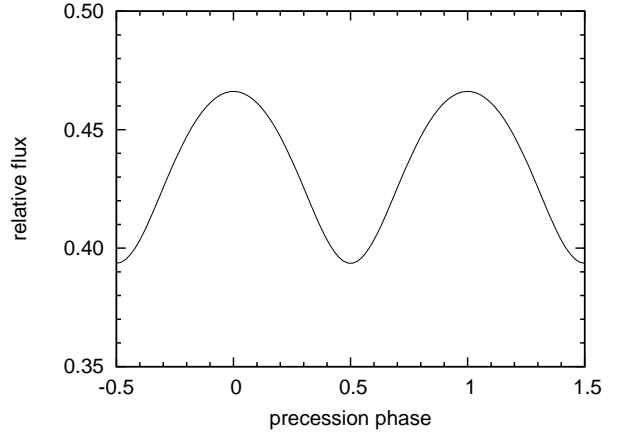
**Figure 7.** *Upper frame:* power spectrum of the values of brightness at minimum light. The strongest signal occurs at 0.2721(10) c d⁻¹, the nodal (N) frequency. The peak labelled with ‘A’ is an alias centred at frequency $1 - N$. *Lower frame:* the values of brightness at minimum light folded on the nodal frequency according to the ephemeris given in Eq. (2).

4.1 The 3.7 d clock

We have estimated the timings of maximum light in the 3.7 d cycle. A total of 27 maxima were timed, with estimated uncertainties on individual timings of ~ 0.1 d. These values are presented in Table 4. A linear regression to these timings provides the following test ephemeris

$$T_{\max}(\text{HJD}) = 2,457,082.01(10) + 3.690(10)E \quad (2)$$

which we used to calculate the $O - C$ diagram shown in Fig. 6. The curvature indicates that no constant period satisfies the data, but rather a period drifting about a mean value of 3.69 d. From a parabolic fit to the $O - C$ residuals, we find that the period drifts at a rate of $dP/dt = -0.0013(2)$, or $dN/dt = 9.5(1.5) \times 10^{-5}$ c d⁻², which amounts to an overall decrease in the nodal period of ~ 0.2 d over the 5 months spanned by our observations.

**Figure 8.** Relative flux, defined as the ratio between the flux at minimum light over the out-of-eclipse flux, as determined from best sinusoidal fits, showing that orbital eclipses are deepest at the minimum of the precession cycle.

4.2 Periodic effect in the eclipse depths

As one may notice in Figs. 1 and 2, the brightness at minimum light (V_{\min}) is notoriously variable, and presumably modulated by the 3.68 d wave discussed earlier for the out-of-eclipse brightness (V_{out}). As for the eclipse depths, variations – if they exist at all – are not easy to perceive from these figures. We tackle these questions next.

We started by considering our estimates of V_{\min} and checked for possible periodic variations, finding the power spectrum shown in the upper frame of Fig. 7. The dominant peak at 0.2721 c d⁻¹ shows that the 3.68 d period also modulates the minimum light. The lower frame of Fig. 7 shows these values folded (and binned) on the ephemeris given in Eq. (2), and indicates that V_{\min} varies essentially as a sinusoid. Comparison with the out-of-eclipse modulation V_{out} indicates that: (i) both share the same periodicity; (ii) V_{\min} has a larger semi-amplitude (0.30 mag) than V_{out} (0.22 mag); and (iii) both are in phase (difference in phase of 0.02 ± 0.03 , according the corresponding best sinusoidal fits).

What about the *eclipse depth*? If this is defined as $\Delta V = V_{\min} - V_{\text{out}}$, our previous analysis shows that ΔV is indeed non-constant, and varies sinusoidally throughout the precession cycle. Adopting our best sinusoidal fits for V_{\min} and V_{out} , the eclipse depth is found to vary, on average, from 0.82 mag at the maximum of the precession cycle (phase $\phi_p = 0$) to 1.00 mag at its minimum ($\phi_p = 0.5$).

The cyclic effect on the eclipse depth can also be analyzed in terms of fluxes. Fig. 8 shows the 3.68 day modulation of the flux at minimum light relative to the out-of-eclipse flux. In line with the discussion above in terms of magnitudes, eclipses are deepest at the minimum of the precession cycle. We note that a similar effect has been reported for the SW Sex nova-like PX And (Stanishev et al. 2002).

4.3 Periodic effect in the mid-eclipse residuals

As we examined the many eclipses, we noticed some which were distinctly asymmetric, confounding the effort to derive a precise timing of mid-eclipse. Departures from the mean ranged up to ~ 80 s, but seemed to be systematic with time.

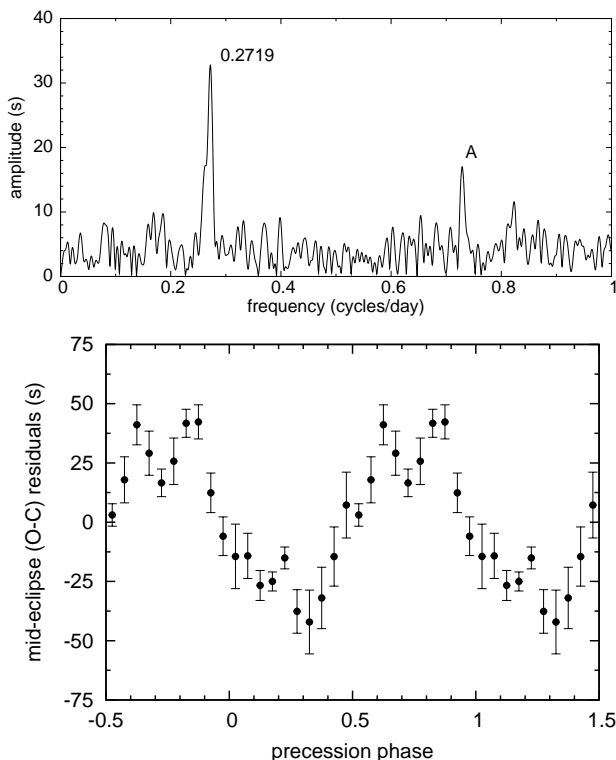


Figure 9. *Upper frame:* power spectrum of the departures of eclipse timings from the ephemeris given in Eq. (1). A significant peak occurs at $0.2719(10) \text{ c d}^{-1}$, the same (nodal) frequency, N , characterizing the large variations in light seen in Fig. 2. The peak labelled with ‘A’ is an alias centred at frequency $1 - N$. *Lower frame:* fold of these residuals on the nodal frequency according to the ephemeris given in Eq. (2), showing a periodic effect with a semi-amplitude of $33.3(9) \text{ s}$.

So we calculated the power spectrum of the departures of eclipse timings from the ephemeris given in Eq. (1), and found the result seen in the upper frame of Fig. 9.

A significant peak is present at $0.2719(7) \text{ c d}^{-1}$, or $3.678(9) \text{ d}$, the same period behind the large variations in light seen in Fig. 2. Apparently the centre of light, or at least the centre of eclipsed light, wanders back and forth on this period. And since the eclipsed light of UX UMa is dominated by the accretion disc, we conclude that the disc’s photometric centre moves about with this period.³ (Presumably the true orbital period, set by the laws of dynamics, can be relied on to stay immovable during this 5-month campaign.) A fold of the residuals on the ephemeris given in Eq. (2) yields the result seen in the lower frame of Fig. 9: a nearly sinusoidal wiggle with a semi-amplitude of $33.3(9) \text{ s}$. It seems that there is no time lag ($O - C = 0$) in the orbital eclipses at precession phases $\phi_p \approx 0$ and 0.5 (maximum and minimum light, respectively). The eclipse takes place earlier than expected (negative residuals) for $0 < \phi_p < 0.5$, and later (positive residuals) for $0.5 < \phi_p < 1$.

³ Where ‘disc’ may or may not include the bright spot arising from mass transfer, which is a well-known permanent feature which causes the large asymmetry in the eclipse centred around orbital phase 0.05 (see Fig. 9 of Nather & Robinson (1974)).

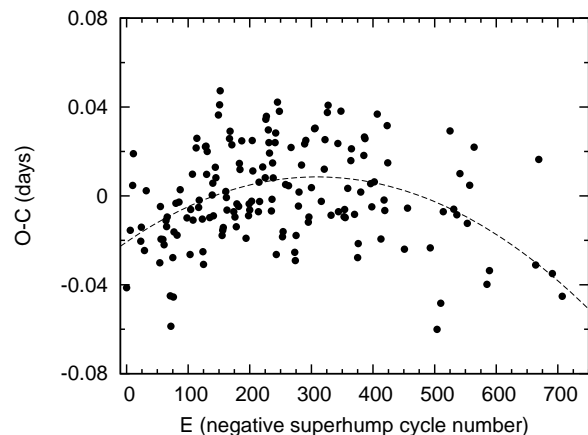


Figure 10. $O - C$ diagram of the 0.1867 d superhump maxima with respect to the test ephemeris given in Eq. (3).

4.4 The 0.1867 day (negative superhump) clock

We tried to time individual maxima in the negative-superhump cycle by picking out local maxima after removing the 3.68 d and orbital signals. Table 5 shows the resultant 161 timings, with errors in individual timings estimated to be around 0.007 d . A linear regression to these timings provides the ephemeris

$$T_{\max}(\text{HJD}) = 2,457,098.499(3) + 0.186700(11)E. \quad (3)$$

The associated frequency, $\omega_{\text{hsh}} = 5.3562(3) \text{ c d}^{-1}$, is fully consistent with the value found from the power spectrum of the out-of-eclipse photometric data. The corresponding $O - C$ residuals relative to the above ephemeris are shown in Fig. 10. The downward curvature of the residuals mirrors that of Fig. 6, verifying that the observed superhump frequency changes in lockstep with the observed precession frequency. From a parabolic fit to the residuals, we find that the period of the negative superhump decreases at a rate $dP_{\text{nsh}}/dt = -3.3(6) \times 10^{-6}$ or $d\omega_{\text{hsh}}/dt = 9.5(1.7) \times 10^{-5} \text{ c d}^{-2}$. The latter agrees with the rate of variation of the nodal frequency we found before, as it should be expected from the relation $\omega_{\text{hsh}} = \omega_{\text{orb}} + N$. We note that this relation remains valid in the short term, not just for the whole season.

The departures from a smooth curve are quite large – up to 45 min – whereas we estimate a typical measurement error of 10–15 min. But the dispersion in timings on individual nights is much smaller, so we suspected that some other effect contributes to that variance. The power spectrum of the residuals about the quadratic fit shows a peak at $0.273(2) \text{ c d}^{-1}$, which indicates that the precession term is responsible for this effect, even though its direct photometric signature – the 3.68 d signal – has been accurately subtracted.

5 DISCUSSION

Most cataclysmic variables show a periodic signal at P_{orb} , either from an eclipse – pretty obvious! – or from some other effect of high or moderate inclination, e.g. the periodic obscuration of the mass-transfer ‘hot spot’ as it wheels around the disc. Many (~ 200) also show a photometric period a few

Table 5. Times of maximum light on the 0.1867 day cycle (HJD – 2,457,000).

98.458	99.604	100.371	100.572	102.773	102.966	103.889	104.476	108.551	108.763	108.935
109.495	109.866	110.437	110.621	110.812	111.710	111.883	112.474	112.643	112.859	113.432
113.791	114.366	114.745	116.786	117.703	117.910	118.486	118.652	119.618	119.809	120.338
120.528	121.453	121.625	121.806	122.419	122.606	122.780	122.977	123.694	124.451	124.643
124.815	125.397	125.579	126.354	126.732	126.925	127.420	127.609	127.797	128.560	128.744
128.925	129.704	129.894	130.448	130.978	131.349	131.718	131.915	132.474	132.680	132.864
133.437	134.700	135.457	135.649	135.833	136.397	136.611	136.784	138.446	138.646	138.824
139.773	140.515	140.728	140.916	141.470	141.651	141.833	142.367	142.559	142.762	142.942
143.518	143.709	143.841	144.283	144.839	145.716	145.905	146.673	147.606	148.370	149.443
149.626	149.824	150.584	150.777	151.536	152.479	152.854	153.564	153.753	154.513	155.473
155.660	157.494	158.442	158.642	159.401	159.591	160.475	162.561	162.717	163.509	164.395
164.585	164.768	165.528	166.474	166.666	167.570	168.484	168.677	169.447	170.397	170.592
170.778	172.438	172.801	173.559	174.523	175.587	176.538	176.720	177.505	177.675	182.677
183.629	190.519	192.536	193.668	194.456	196.546	197.631	198.562	199.514	201.732	202.496
203.820	207.679	208.432	222.437	223.418	227.474	230.451				

percent longer than P_{orb} (positive superhumps). Most of the latter are short-period dwarf novae, which sprout these signals for 1–4 weeks, during their long outbursts (‘supermaxima’). This is now understood as arising from the apsidal precession of the accretion disc, rendered eccentric at the 3:1 resonance in the disc. A few stars which are not dwarf novae also show this effect, but these are all short-period (< 3.5 h) nova-like variables, which in many ways can be seen as permanently erupting dwarf novae. These signals are known as ‘permanent’ superhumps (Patterson & Richman 1991).

Only a disc large enough to reach the 3:1 resonance can suffer this instability (Whitehurst & King 1991; Lubow 1991), and that is presumably the reason that positive superhumps are only found in short-period stars. But some stars show photometric signals with $P < P_{\text{orb}}$ – the negative superhumps. Much less is known about them. The early papers on these phenomena (Bonnet-Bidaud, Motch & Mouchet 1985; Patterson et al. 1993; Harvey et al. 1995) postulated the existence of a tilted accretion disc, which is forced to precess slowly backwards (relative to the orbit) by the torque from the secondary. The angular relation between the secondary (including its structures, viz. the mass-transfer stream) and the disc then repeats with a period slightly less than P_{orb} . This is a negative superhump. Roughly 20 CVs show negative superhumps (see Table 2 of Montgomery (2009)), and roughly half of these (see Table 5 of Armstrong et al. (2013)) also show a photometric signal at the postulated precession period. Detection of that low-frequency signal is a strong point in support of the theory, since a wobbling disc should present an effective area which varies with the wobble period.

Our data demonstrate that UX UMa joins this club. We hypothesize that its accretion disc wobbles about the orbital plane with a period $P_{\text{nodal}} = 3.68$ d, and we see its effective area varying on that period. But the orbiting secondary – not in the inertial frame! – sees the disc with a slightly shorter recurrence period, such that $1/P_{\text{nsh}} = 1/P_{\text{orb}} + 1/P_{\text{nodal}} = 5.356 \text{ c d}^{-1}$, or $P_{\text{nsh}} = 0.1867$ d. The effect is basically identical to the famous tropical/sidereal year effect in the Earth-Sun system, or the draconic/sidereal month effect in the Earth-Moon system. Montgomery (2009) discusses this analogy in great, and fascinating, detail.

The cause and maintenance of disc tilt is not known.

No actual dwarf nova in outburst shows negative superhumps, although their closest cousins – nova-like variables with $P_{\text{orb}} < 3.5$ h – frequently do (Patterson et al. 1993; Armstrong et al. 2013). It’s possible that the 3:1 resonance is again involved, but with the tilt instability growing so slowly that only a ‘permanent’ dwarf nova, which is in a high-viscosity state for a long time, can develop sufficient tilt. An alternative theory is the recent work by Thomas & Wood (2015), which invokes white-dwarf magnetism to break the azimuthal symmetry and permit – in fact, create – disc tilt. They make an impressive case; and such an origin would be especially intriguing because UX UMa also shows the very-high-frequency DNOs (signatures of white-dwarf rotation?), which have remained equally mysterious.

UX UMa is not a typical member of this club. Most members belong to the SW Sex subclass, which have shorter P_{orb} (3–4 h), occasional excursions to very low states, and only the $\omega_{\text{orb}} + N$ feature (lacking N , and emphatically lacking $2\omega_{\text{orb}} + N$). They also commonly show periodic radial-velocity signals of high amplitude, presumably indicative of the mass-transfer stream overflowing the disc (because of the tilt). Maybe CV zoology needs to be adjusted somewhat, in order to fit these oddities.

Finally, why did we find all these new effects in a star which has been closely studied for 60 years? Did they first arise in 2015? It seems unlikely. Inspection of early light curves (Walker & Herbig 1954; Johnson, Perkins & Hiltner 1954) reveals that both the mean brightness and eclipse depths are not constant (see, for instance, Table 1 in Smak (1994)), with variations within the range we have observed in 2015. Also, Knigge et al. (1998b) have reported differences of up to 50 per cent in brightness in *Hubble Space Telescope* (*HST*) observations of UX UMa carried out 3 months apart in 1994. They infer that a substantial (~ 50 per cent) variation of the mass transfer rate must have occurred, but a precessing disc during the 1994 *HST* observations would also account for the observed brightness variations. We therefore believe that the mean brightness and eclipse depths were not exceptional in 2015. We selected the star for observation partly because previously published light curves showed variations in the orbital waveform – suggesting that a signal at some nearby frequency might be present. But to actually reveal these effects, an extensive campaign is required, and

no such campaign has ever been reported. So it's a decent bet, though by no means sure, that these superhump effects have been lurking, unsuspected, in many previous observations of UX UMa.

6 SUMMARY

(1) We report a long photometric campaign during 2015, with coverage on 121 of 150 nights, totalling ~ 1800 h. The star displayed a sinusoidal signal with a semi-amplitude of 0.22 mag and a mean period of 3.680(7) d, or a frequency 0.2717(5) c d^{-1} . We identify the latter as N , the accretion disc's (putative) frequency of retrograde nodal precession.

(2) Fig. 1 shows that the orbital waveform is highly variable from day to day, but not from orbit to orbit. Power-spectrum analysis shows that this arises from signals non-commensurate with P_{orb} , namely 'negative superhumps' with frequencies $\omega_{\text{orb}} + N$ and $2\omega_{\text{orb}} + N$.

(3) The mean orbital light curve – shown in Fig. 3 and summed over more than 200 orbits – shows a wave with maximum light around orbital phase 0.35. This is roughly 180° out of phase with the hot-spot effect seen in U Gem, which defines the standard accretion geometry for CVs.

(4) The 3.68 d period is strongly manifest in essentially every quantity we studied. The eclipse times wobble on this period with an amplitude of 33.3(9) s, probably because the disc's (projected) centre of light moves with that period. The superhump times also wobble with that period, as do the eclipse depths.

(5) Fig. 6 shows that the precession period varied smoothly, decreasing by ~ 0.2 d over the 5-month campaign. As it did, the superhump period changed accordingly, maintaining $\omega_{\text{sh}} = \omega_{\text{orb}} + N$.

(6) About a dozen other CVs show this basic triad of frequencies (ω_{orb} , N , and $\omega_{\text{orb}} + N$). Most are so-called SW Sex stars. Because the physics which underlies this category is probably the wobbling non-coplanar disc, it is likely that the credentialing scheme of that club (Thorstensen et al. 1991; Rodríguez-Gil et al. 2007; Dhillon, Smith & Marsh 2013) will have to change, in order to accommodate UX UMa. We note that Neustroev et al. (2011) has also, based on spectroscopic evidence, proposed that UX UMa has transient episodes of SW Sex behaviour.

ACKNOWLEDGMENTS

We thank the National Science Foundation for support of this research (AST12-11129), and also the Mount Cuba Astronomical Foundation. Finally, we thank the American Association of Variable Star Observers (AAVSO) for providing the infrastructure and continued inspiration which makes programs like this possible.

REFERENCES

Armstrong E., Patterson J., Michelsen E., Thorstensen J.R., Uthas H., Vanmunster T., Hamsch F.-J., Roberts G., Dvorak S., 2013, MNRAS, 435, 707
 Baptista R., Horne K., Hilditch R.W., Mason K.O., Drew J.E., 1995, ApJ, 448, 395

Baptista R., Horne K., Wade R.A., Hubeny I., Long K.S., Rutten R.G.M., 1998, MNRAS, 298, 1079
 Bonnet-Bidaud J.M., Motch C., Mouchet M., 1985, A&A, 143, 313
 Dhillon V.S., Smith D.A., Marsh T.R., 2013, MNRAS, 428, 3559
 Harvey D., Skillman D.R., Patterson J., Ringwald F.A., 1995, PASP, 107, 551
 Henden A.A., Levine S.E., Terrell D., Smith T.C., Welch D., 2012, JAAVSO, 40, 430
 Johnson H.L., Perkins B., Hiltner W.A., 1954, ApJS, 1, 91
 Knigge C., Drake N., Long K.S., Wade R.A., Horne K., Baptista R., 1998a, ApJ, 499, 429
 Knigge C., Long K.S., Wade R.A., Baptista R., Horne K., Hubeny I., Rutten R.G.M., 1998b, ApJ, 499, 414
 Krzeminski W., Walker M.F., 1963, ApJ, 138, 146
 Lenz P., Breger M., 2005, Commun. Asteroseismol., 146, 53
 Linnell A.P., Godon P., Hubeny I., Sion E.M., Szkody P., 2008, ApJ, 688, 568
 Lubow S.H., 1991, ApJ, 381, 268
 Montgomery M.M., 2009, ApJ, 705, 603
 Nather R.E., Robinson E.L., 1974, ApJ, 190, 637
 Neustroev V.V., Suleimanov V.F., Borisov N.V., Belyakov K.V., Shearer A., 2011, MNRAS, 410, 963
 Paczynski B., Schwarzenberg-Czerny A., 1980, Acta Astron., 30, 127
 Patterson J., 1981, ApJS, 45, 517
 Patterson J., 2011, MNRAS, 411, 2695
 Patterson J., Richman H., 1991, PASP, 103, 735
 Patterson J., Thomas G., Skillman D.R., Diaz M.P., 1993, ApJS, 86, 235
 Patterson J., et al., 2002, PASP, 114, 721
 Rodríguez-Gil P., et al., 2007, MNRAS, 377, 1747
 Skillman D.R., Patterson J., 1993, ApJ, 417, 298
 Smak J., 1971, Acta Astron., 21, 15
 Smak J., 1994, Acta Astron., 44, 59
 Stanishev V., Kraicheva Z., Boffin H.M.J., Genkov V., 2002, A&A, 394, 625
 Thomas D.M., Wood M.A., 2015, ApJ, 803, 55
 Thorstensen J.R., Ringwald F.A., Wade R.A., Schmidt G.D., Nor-sworthy J.E., 1991, AJ, 102, 272
 Walker M.F., Herbig G.H., 1954, ApJ, 120, 278
 Warner B., Nather R.E., 1971, MNRAS, 152, 219
 Warner B., Nather R.E., 1972, MNRAS, 159, 429
 Whitehurst R., King A., 1991, MNRAS, 249, 25
 Zverev M.S., Kukarkin B.V., 1937, Variable stars, 5, 125

This paper has been typeset from a $\text{\TeX}/\text{\LaTeX}$ file prepared by the author.